JOURNAL OF MATERIALS SCIENCE, 30 (1995) 1939–1948

Preparation and properties evaluation of zirconia-based/Al_2O_3 composites electrolytes for solid oxide fuel cell systems

Part II *Sintering behaviour and microstructural development*

L. M. NAVARRO, P. RECIO, P. DURAN
Instituto de Cerámica y Vidrio (CSIC), Electroceramics Department, 28500 Arganda del Rey, Madrid, Spain

The compaction behaviour of ultrafine yttria-doped zirconia powders (6–8 nm) without and with alumina additions (0 to 20 wt%) has been studied. From the pore size distribution and using isothermal and nonisothermal techniques, the sintering behaviour of zirconia compacts in the temperature range 800–1500 °C was studied. It was found that alumina additions (up to 10 wt%) enhanced the zirconia compacts' densification process and, above that alumina content, that process was retarded. Alumina additions did not affect the grain grown process in tetragonal zirconia samples. However, this was strongly hindered in the fully stabilized zirconia ones. The results were compared with those obtained in the same experimental conditions on a commercial zirconia powder.

1. Introduction

As previously described in several papers [1–5] the achievement of Y_2O_3-doped zirconia dense ceramics with improved mechanical and electrical properties is very difficult. In the low Y_2O_3 concentration (2–3 mol %), the solid solution formed has a tetragonal structure (Y-TZP) and its stability is strongly governed by a critical grain size above which the zirconia phase is spontaneously transformed to a monclinic one [6]. When tetragonal zirconia stable at room temperature is achieved an ageing phenomenon at low temperature ($\leqslant 500$ °C) is present which strongly degrades both the strength and the electrical conductivity of the fabricated material. The requirements for low-temperature tetragonal zirconia stability are much more rigorous when the ceramic has to be used in hot water, and although it is true that many attempts have been carried out to avoid such degradation properties [7–9], the final result is a material presenting a compromise between these properties being slightly worse and a better resistance to ageing degradation.

In the case of fully stabilized zirconia (FSZ), with a high ionic conductivity, the problem is how to obtain dense bodies sintered at a temperature as low as possible, with small and uniform grain size and with a good mechanical strength and thermal shock resistance. By using chemical precursors it is possible to achieve calcined powders with a controlled and small particle size, allowing sintering at low temperatures [4, 10, 11]. However, the formation and sintering of cubic zirconia ceramics run parallel to a rapid grain growth process which is detrimental to the final density of the sintered bodies which are to be used as electrolytes in SOFC systems.

In view of the difficulties of fulfilling the grain size requirement in the case of FSZ materials, several methods of obtaining a fine-grained ceramic have been tried and, as a result, it is believed that inclusions of alumina in the zirconia matrix could be a suitable additive. Although in the past decade many papers [12–16] have been devoted to the study of the Al_2O_3 effect on the tetragonal zirconia transformation and on its properties, there is no exhaustive study of its influence on both the densification and the grain growth processes of zirconia-based ceramics. The present work, which is the second part of a series, was undertaken to study the effect of Al_2O_3 additions on the compaction behaviour of both commercial and co-precipitated Y-doped zirconia powders, their sintering behaviours, and their microstructural development.

2. Experimental procedure

Zirconia powders containing different amounts of yttrium and alumina were synthesized by a gel-precipitation method using Zr and Y chlorides and Al nitrate as precursor chemicals. The details of the powder preparation, which is a modification of the Van de Graaf *et al.* [4] synthesis method, have been described elsewhere [18].

Green compacts were prepared by isostatic pressing at 200 MPa of the synthesized powders. The pore size distribution and the pore volume in the compacts were calculated from a nitrogen adsorption/desorption isotherm at 77 K using an Accusorb 2100 E

0022–2461

Micromeritics, and by mercury porosimetry using a Micromeritics Autopore II 9215 model. After pressing, the compacts were sintered at 1200–1600 °C for 2 h in air atmosphere. For the samples with tetragonal symmetry, the highest sintering temperature was 1400 °C. The shrinkage behaviour study was performed using a high temperature dilatometer (Adamel-Lhomargy-2D) at heating and cooling rates of 5 °C min^{-1}. The density of the sintered samples was determined using the immersion Archimedes method with water. X-ray diffraction analyses were carried out on the as-sintered and polished surfaces, and the lattice parameters were also calculated. Microstructural evaluation was carried out using scanning electron microscopy (Karl Zeiss 450E), and the grain size was measured by the interception method [19].

3. Experimental results

3.1. Powder compaction

The consolidation of commercial zirconia powders with or without alumina additions by isopressing at 200 MPa resulted in compacts which had two peaks in the pore size distribution, one at a pore diameter of about 4 nm, and the other at a pore diameter of about 45 nm (see Fig. 1), and a density of 45% theoretical density and somewhat lower with alumina additions. In the case of the coprecipitated zirconia powders the green compacts had a rather narrow size distribution and a peak in the pore size distribution at a pore diameter much smaller, ~ 8 nm. However, the green density of the zirconia compacts was in this case about 43% theoretical density, and this density value was lowered up to 39% with alumina additions.

Figs 2 and 3 show the green microstructure of both the commercial and the coprecipitated fracture surfaces of the compacted samples. All of them presented a uniform microstructure corresponding to powders with a low agglomeration level. Only in the case of the Z-4Y coprecipitated samples was a different microstructure present, and it is was assumed to be a consequence of the dense crystallite packing. The average crystallite size of this samples was less than 6 nm.

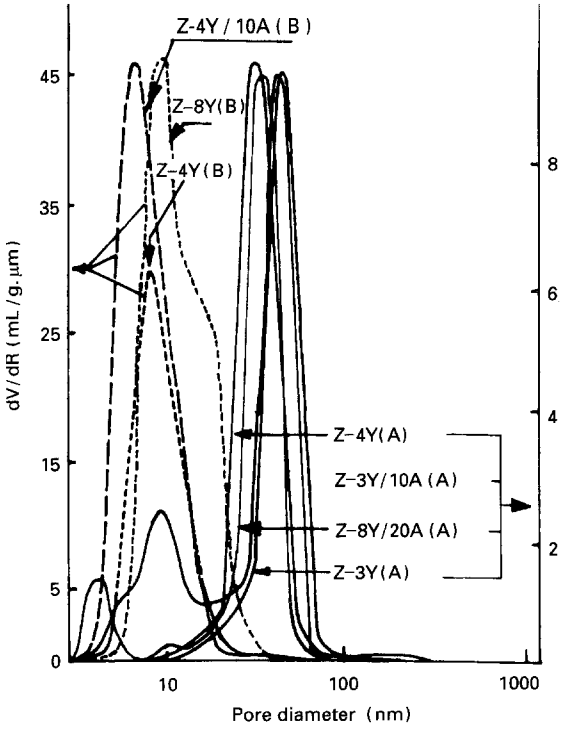

Figure 1 Pore size distribution of green compacts: (a) commercial powder, (b) coprecipitated powder

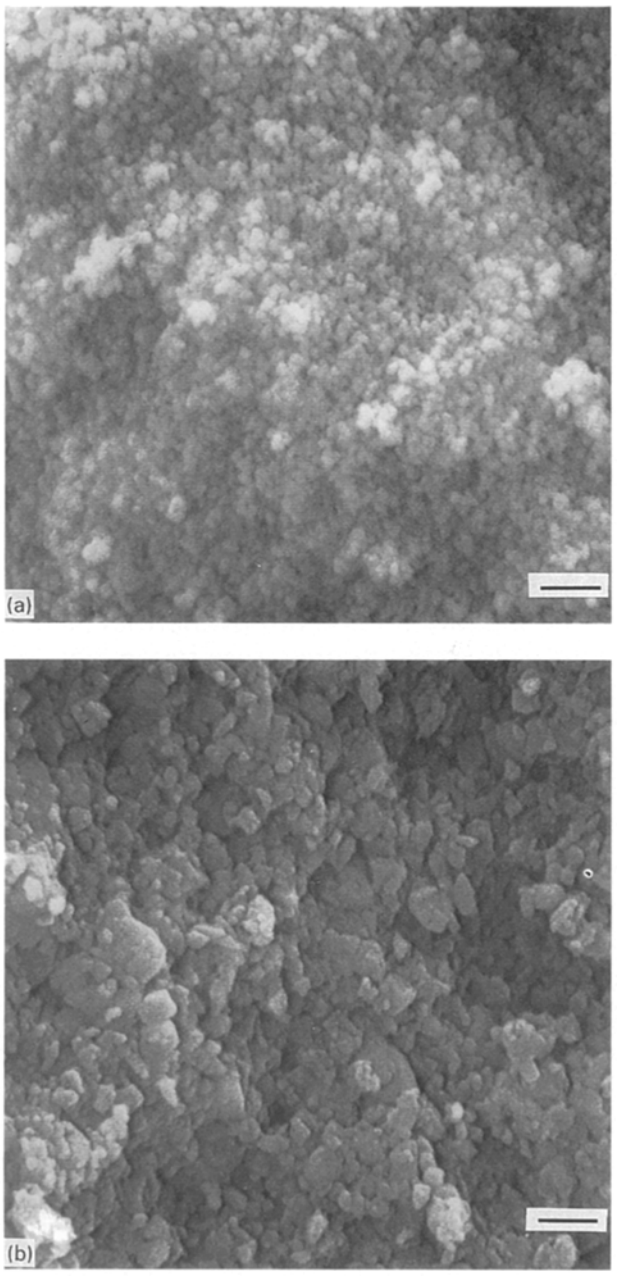

Figure 2 Fracture surface of Z-8Y commercial green compacts: (a) without alumina, (b) with 10 % Al_2O_3 (bar = 1 μm)

3.2. Sintering

In order to determine both the optimum sintering temperature and the alumina content, the sintering experiments were carried out between 1200 and 1600 °C on the two kinds of zirconia powders with and without alumina. As shown in Fig. 4, the sintering densities increased as the alumina content increased up to a maximum at 10 wt% Al_2O_3 and then decreased. This trend was similar in all the zirconia series in that sintering temperature range.

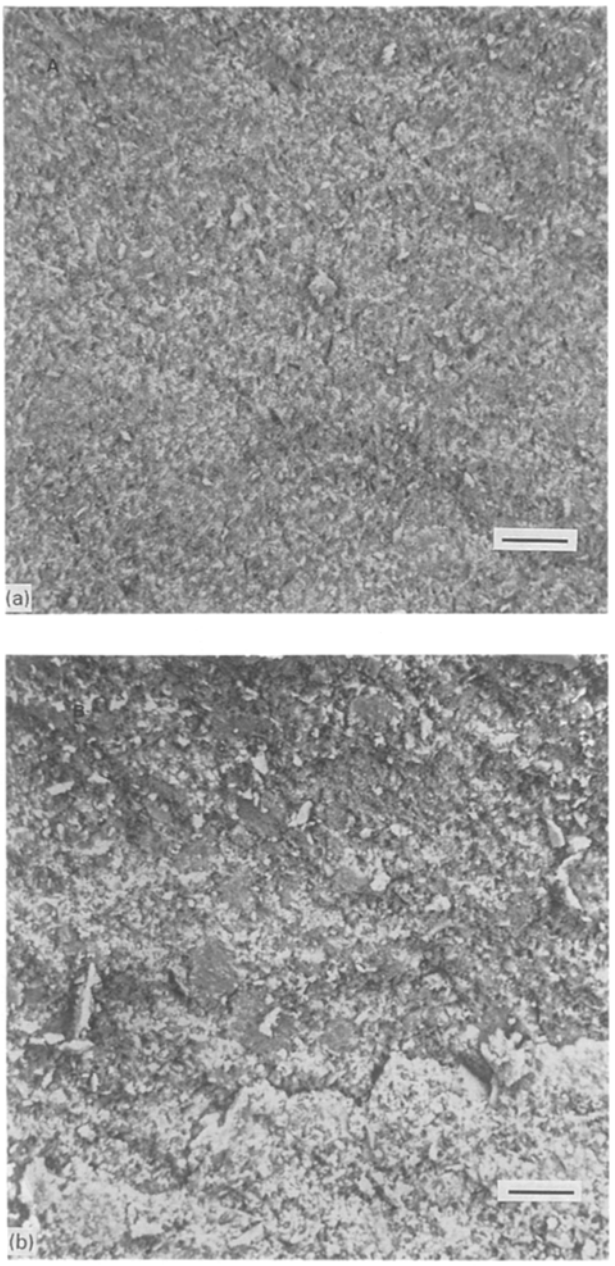

Figure 3 Fracture surface of Z-8Y coprecipitated green compacts: (a) without alumina, (b) with 10% Al_2O_3 (bar = 20 μm)

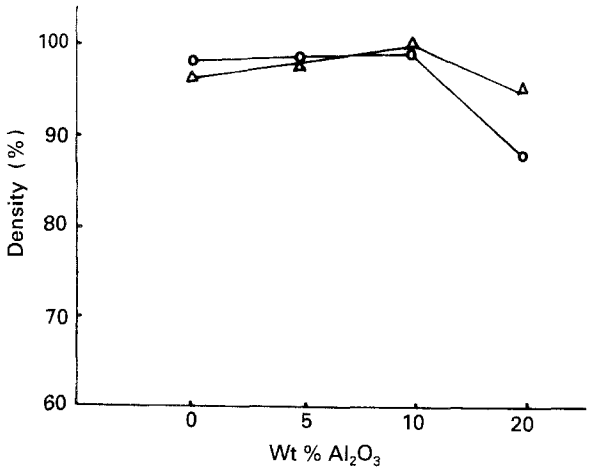

Figure 4 Influence of alumina additions on the densification of commercial zirconia samples, 1400 °C, 2 h; ○—○ Z-4Y; △—△ Z-6Y

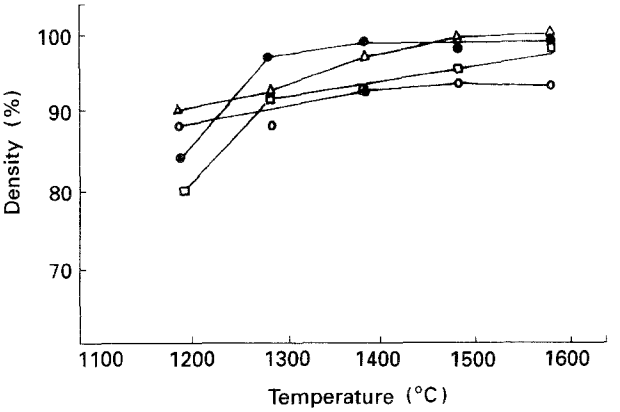

Figure 5 Densification as a function of temperature of Z-8Y samples; (●, □) commercial, (○, △) coprecipitated powders, □—□ Z-8Y; ●—● Z-8Y/10A; ○—○ Z-8Y; △—△ Z-8Y/10A

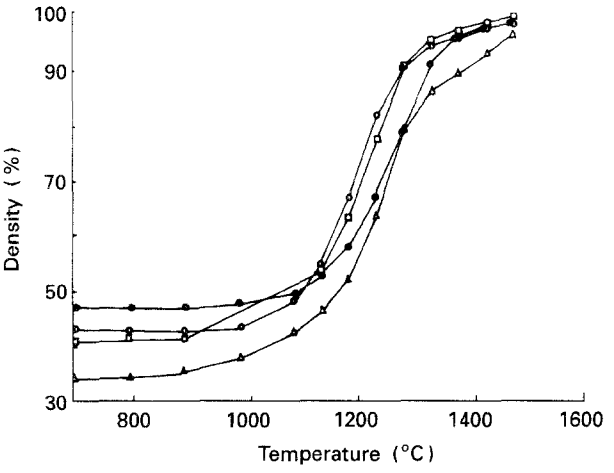

Figure 6 Dilatometric curves of commercial zirconia samples as a function of the alumina additions. ●—● Z-4Y; ○—○ Z-4Y/5A; □—□ Z-4Y/10A; △—△ Z-4Y/20A

Fig. 5 shows the density variation for both commercial and coprecipitated Z-8Y samples without and with 10 wt% Al_2O_3 as a function of the sintering temperature. As can be seen, at 1200 °C commercial zirconia samples yielded low sintering densities, but with increasing sintering temperature the densification degree increased, and the best densification was achieved at a sintering temperature of 1600 °C (~ 95% dense). In the case of the samples containing 10 wt% Al_2O_3 a saturation value (~ 98% of the theoretical density) was reached at 1400 °C.

In the case of the coprecipitated Z-8Y samples, a high densification level (~ 90% dense) was achieved at a temperature as low as 1200 °C. However, the best densification conditions were not achieved up to 1500 °C (~ 93% dense) for Z-8Y without alumina and ~ 99% dense for Z-8Y containing 10 wt% Al_2O_3.

The sintering behaviour of the powder compacts was also investigated by dilatometry. From the dilatometric curves (Fig. 6), all the commercial powder compacts independently of the Y_2O_3 content started to sinter at about 1000 °C and, up to 1500 °C (the end point of the dilatometer), the compacts densified to about 98% theoretical density. Compared with the coprecipitated powder compacts (Fig. 7a and b),

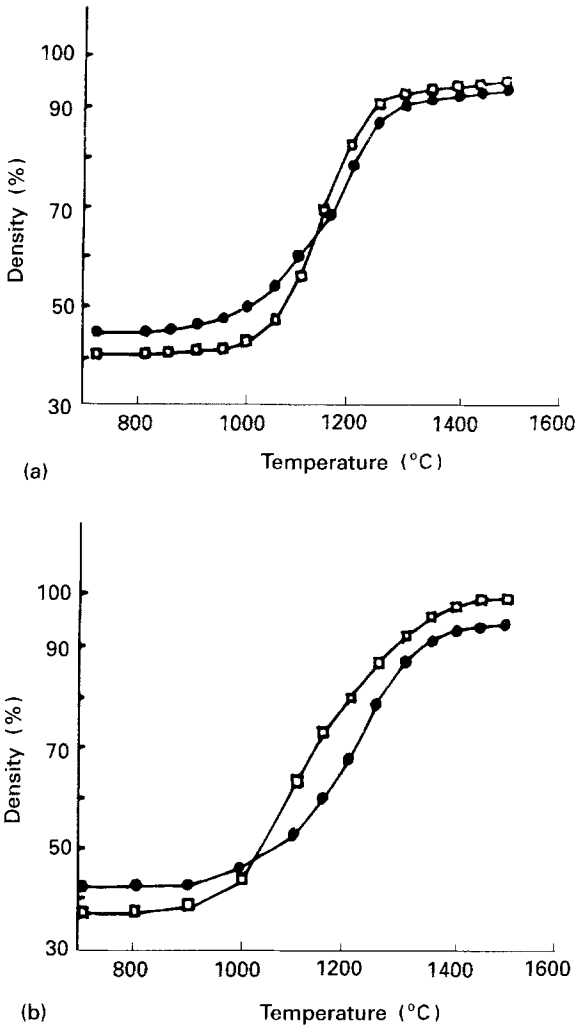

Figure 7 Dilatometric curves of zirconia samples: (a) commercial ●—● Z-4Y, □—□ Z-4Y/10A; (b) coprecipitated powders, ●—● Z-8Y, □—□ Z-8Y/10A

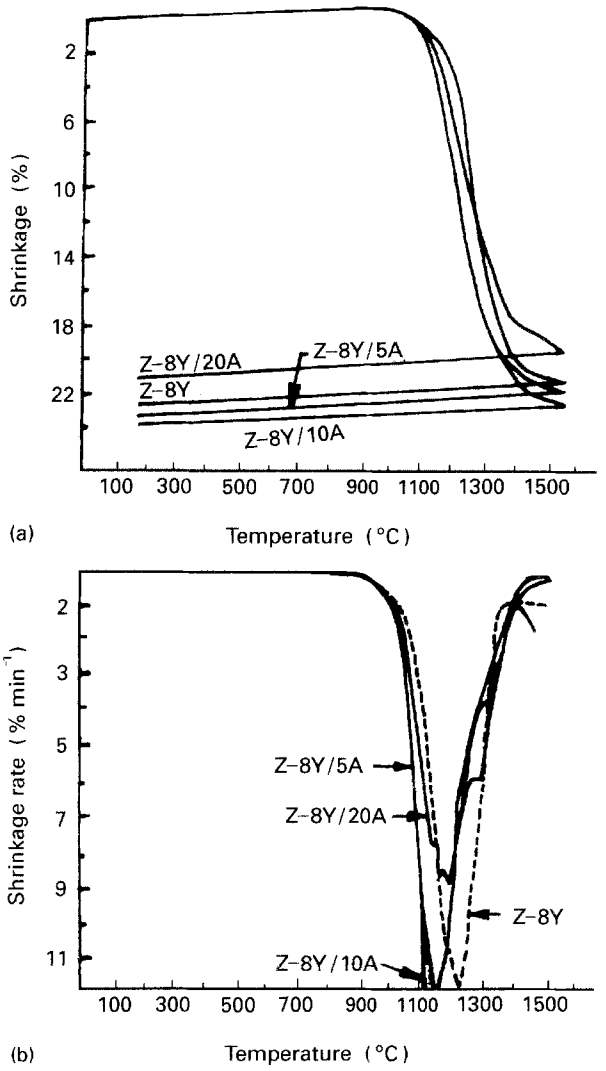

Figure 8 (a) Shrinkage behaviour and (b) shrinkage rate of commercial zirconia composites

a much broader sintering interval exists for those powder compacts, which indicates a high sintering activity but also a higher particle size. The shape of the densification curves is the same and this probably means that the densification process mechanism is also the same for the two kinds of powder compacts.

It can be observed that the starting densification temperature is lower for the coprecipitated powder compacts, and it could be correlated to the smaller crystallite size of the starting powders. Thus, densification of the coprecipitated powder compacts starts at a temperature (~ 800 °C) lower than that of the commercial ones, and the densification from 50 to 95% occurs in a temperature region of about 270 °C, which is much narrower than in the case of the commercial powder compacts (~ 350 °C). This difference in sinterability was more pronounced in the case of the same composition containing 10 wt% Al_2O_3. Thus, in the coprecipitated compacts, that densification level was achieved between 1080 and 1240 °C, and between 1070 and 1310 °C for the commercial compacts; see Figs 6 and 7a. Such different densification behaviour may only be explained by a green aggregate–agglomerate structure strongly different in both powder compacts, which is responsible for the correct elimination of the intra- and inter-agglomerate pores.

3.3. Shrinkage behaviour

Fig. 8a shows the shrinkage behaviour of the commercial zirconia Z-8Y samples containing 0 to 20 wt% Al_2O_3 in a dilatometer at a heating rate of 5 °C/min, and Fig. 8b shows the shrinkage rate curves for the same zirconia samples. It can be observed that in all the samples the shrinkage starts at the same temperature (~ 900 °C), independently of the Al_2O_3 content. This fact indicates that the presence of Al_2O_3 does not affect the shrinkage behaviour of the zirconia samples in the first densification steps. As the temperature increased a strong shrinkage was present between 1000 and 1325 °C, and this was higher for the Z-8Y/10A samples (~ 24%) than for the Z-8Y/20A samples (~ 21%), which is in agreement with the results of Fig. 4. On the other hand, the shrinkage rate was also higher (see Fig. 8b) for the sample containing 10 wt % Al_2O_3 than for the other zirconia samples, and the maximum shrinkage rate was achieved at a lower temperature (~ 1150 °C) against 1210 °C for the Z-8Y/20A sample.

A more detailed dilatometric study was carried out on the Z-8Y/20A commercial sample and, as can be seen in Fig. 9, no shrinkage occurred during heat-up to 1000 °C and about 18 % of the total took place at

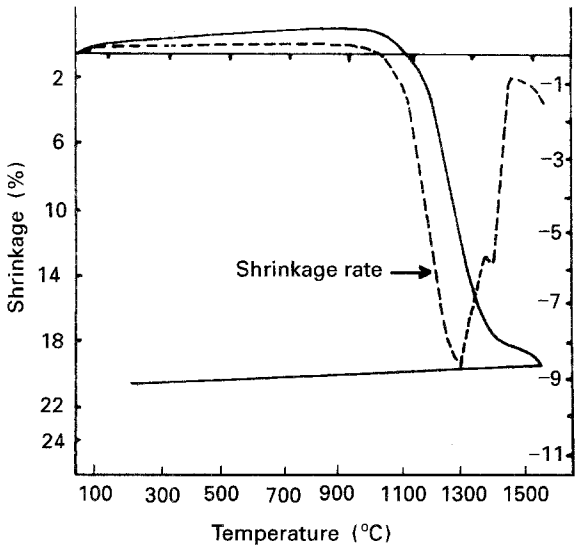

Figure 9 Detailed shrinkage behaviour of commercial Z-8Y/20A composites

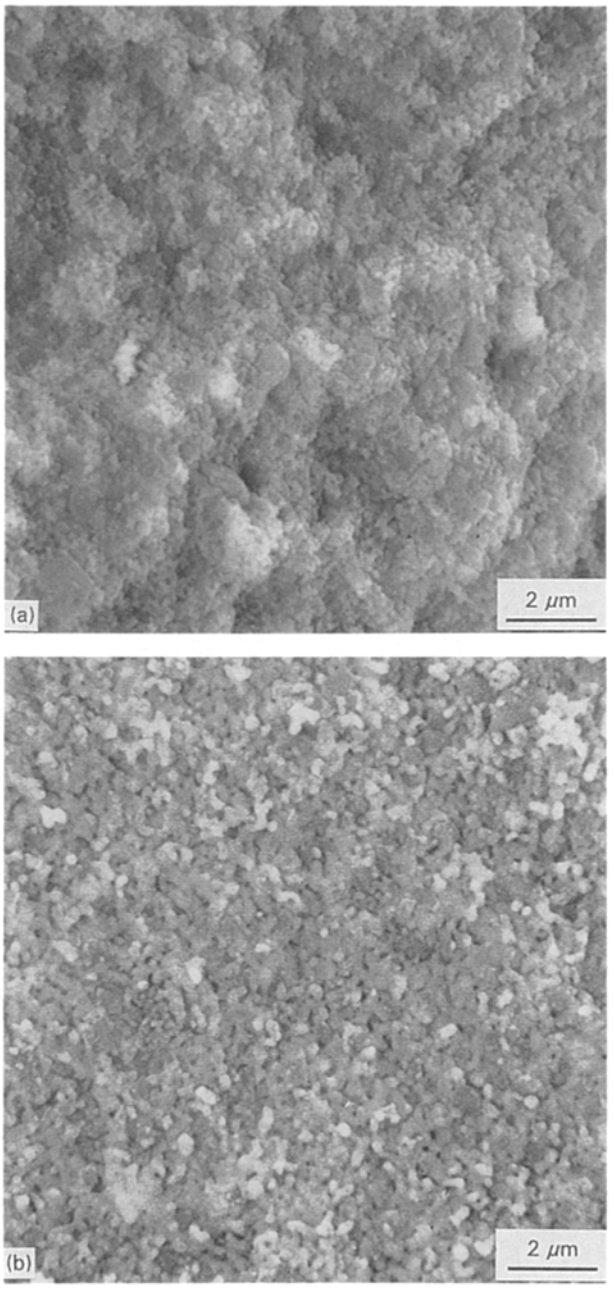

Figure 10 Microstructural evolution of the Z-8Y/20A commercial composite during densification

1297 °C. Above that temperature and up to the end of the sintering process (1500 °C), only a shrinkage of about 2% more occurred. Such sintering behaviour was coincident with the shrinkage rate results shown in Fig. 9. When the compact was heated at 5 °C/min, shrinkage started at about 960 °C, reached a maximum rate at 1209 and 1297 °C, and showed a minimum rate at 1290 °C and around 1400 °C when temporary cessation of the shrinkage rate was observed, and then the shrinkage rate increased again with the rise in temperature.

Fig. 10 shows the microstructure evolution of the Z-8Y/20A sample at the maximum shrinkage rate temperatures 1209 and 1297 °C, which corresponds quite well with a densification level of 60 and 80%, respectively.

In the case of the coprecipitated zirconia samples, shrinkage starts at a temperature 200–250 °C lower than that of the commercial zirconia ones, and the start of shrinkage depends on the Y_2O_3 content. Thus, shrinkage started at 800, 850 and 900 °C for the zirconia samples containing 4, 6 and 8 mol% Y_2O_3 respectively (see Fig. 11a). In the same way (see Fig. 11b), the shrinkage rate maximum was displaced from 1147 °C for the Z-3Y and Z-4Y samples to 1164 °C for the Z-6Y samples, and up to 1240 °C for the Z-8Y sample. On the other hand, the shrinkage was also

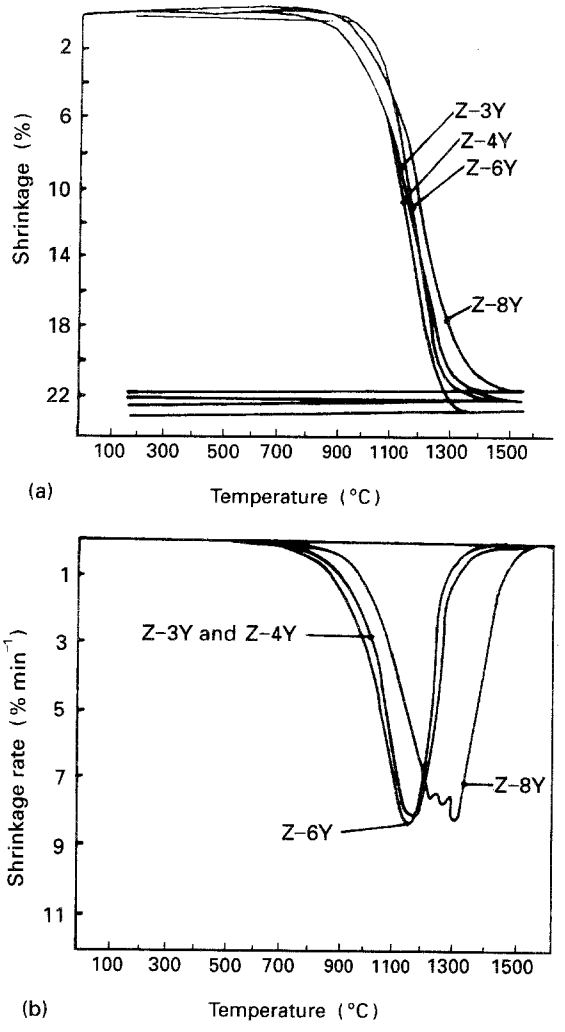

Figure 11 (a) Shrinkage behaviour and (b) shrinkage rate of coprecipitated zirconia samples

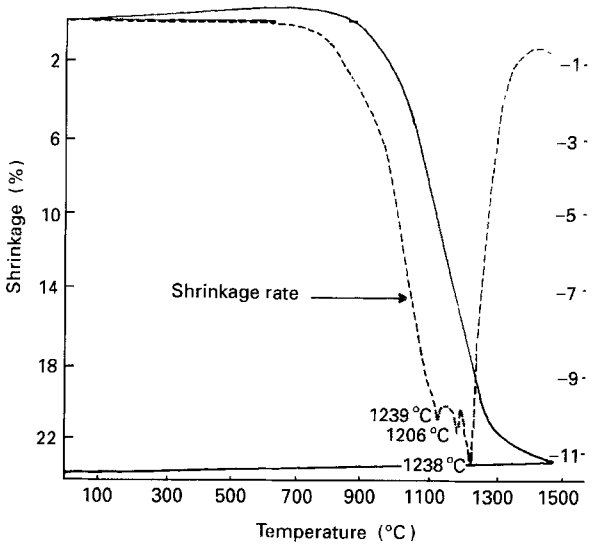

Figure 12 Detailed shrinkage behaviour of Z-8Y coprecipitated sample

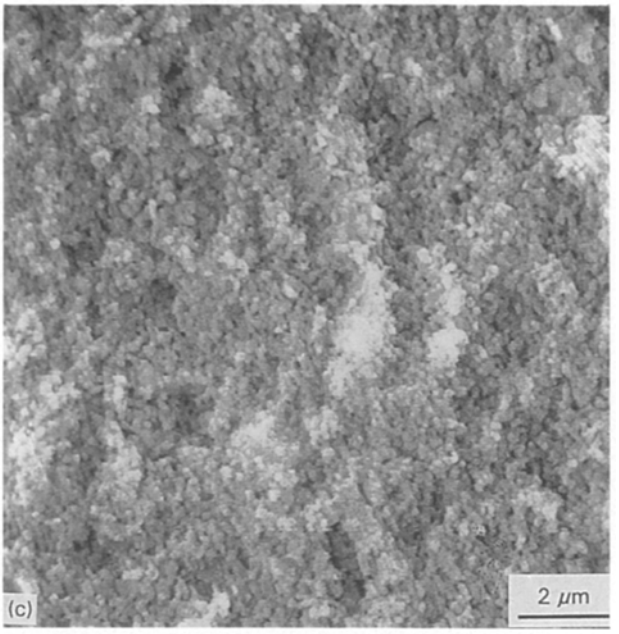

Figure 13 Microstructural evolution of Z-8Y coprecipitated sample during densification. (a) 1133 °C (b) 1205 °C, and (c) 1240 °C

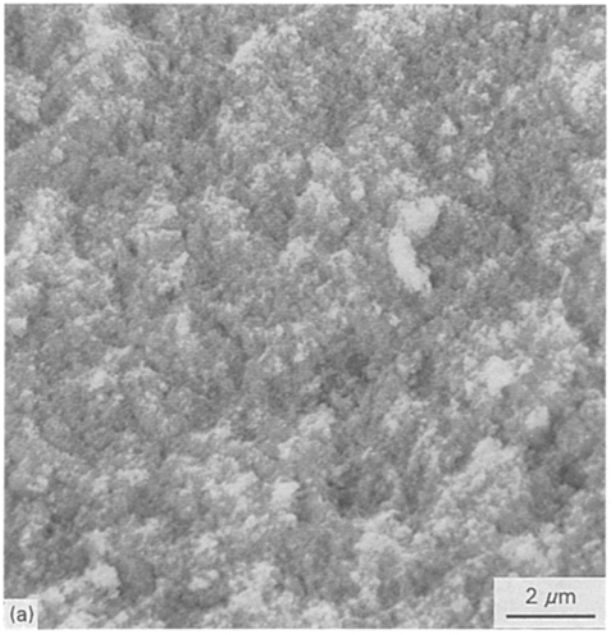

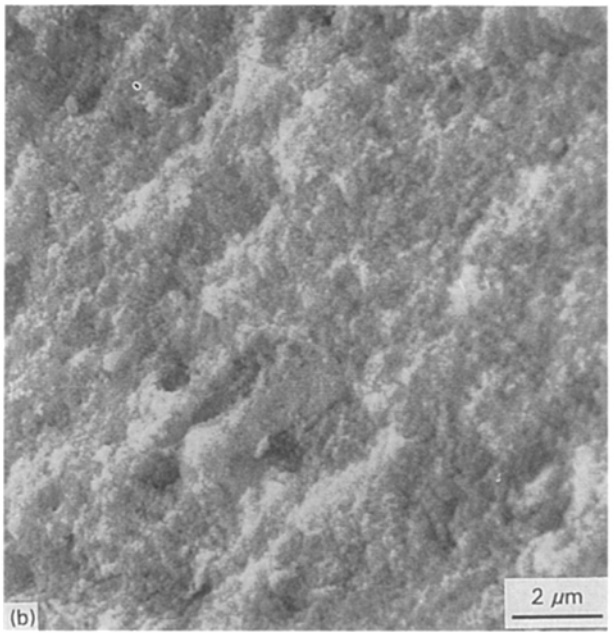

different, being higher for the Z-3Y and Z-4Y samples than for the other zirconia samples. It must also be mentioned that the maximum shrinkage rate was displaced towards lower temperatures for those compositions containing 10 wt % Al_2O_3.

A detailed study of the shrinkage behaviour and the microstructural development, similar to that carried out on the Z-8Y/20A commercial sample, was done on the Z-8Y coprecipitated zirconia sample. As shown in Fig. 12, the shrinkage rate curve shows three maxima at approximately 1137, 1205 and 1240 °C. The compact sample started to shrink at a temperature near 700 °C and showed a first maximum at 1137 °C. Between 1137 and 1200 °C the shrinkage rate remained constant and at 1200 °C a second shrinkage rate maximum appeared. Then the shrinkage rate decreased and a minimum was present at about 1230 °C. Above that temperature the shrinkage rate increased again and a third maximum at 1258 °C was reached. Above 1240 °C the shrinkage rate decreased again up to 1400 °C, when it became minimum. At temperatures higher than 1400 °C the sample shrank slightly up to the end of the sintering process.

The microstructural developments at the different shrinkage rate maxima are shown in Fig. 13. As can be observed, at 1137 and 1205 °C a rearrangement of the zirconia particles occurred with a slight densification. At 1240 °C a densification of about 95% theoretical density was achieved and some sintering necks between the powder particles were present. An incipient grain growth process can also be observed, and grains of about 0.15 μm could be measured.

3.4. Microstructural characterization

Fig. 14 shows an evolution of the microstructure of the commercial zirconia samples without alumina and sintered at 1400 °C for 2 h as a function of the Y_2O_3

content. As can be observed, a uniform grain size distribution occurred in the samples with tetragonal symmetry (Fig. 14a), and a grain size of about 0.4 μm was measured for the Z-3Y sample. With a higher Y_2O_3 content, Z-6Y in Fig. 14b, a bimodal grain size was present as a consequence of the presence of two phases, tetragonal + cubic zirconia, in the sample. Finally, the microstructure of Fig. 14c corresponds to a cubic stabilized zirconia Z-8Y sample in which an exaggerated grain growth had occurred, and the measured average grain size was about 3.5 μm.

Additions of alumina to the above zirconia samples clearly inhibited the grain growth except in the case of the tetragonal zirconia sample. Fig. 15 shows the grain growth process of the commercial zirconia samples as a function of the alumina content. It must be observed that the influence of alumina additions in inhibiting the zirconia grain growth process is stronger at the low alumina content ($\leqslant 5$ wt % Al_2O_3). For higher

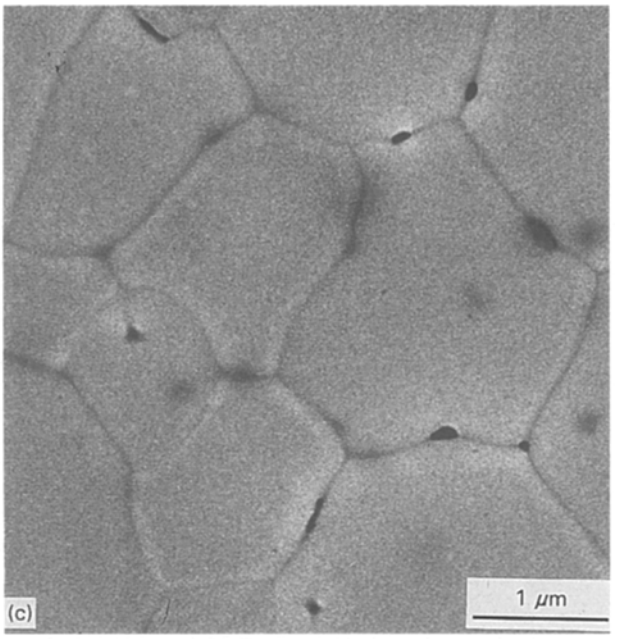

Figure 14 Microstructure of commercial zirconia samples sintered at 1400 °C as a function of Y_2O_3 content. (a) 3 mol %, (b) 6 mol %, (c) 8 mol %

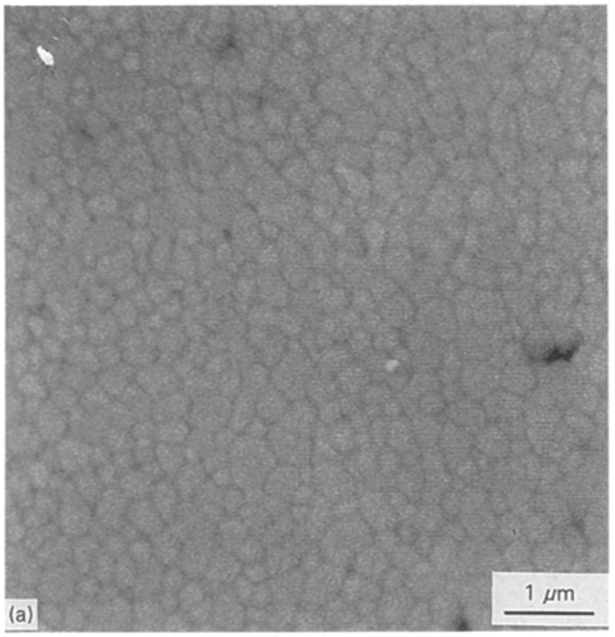

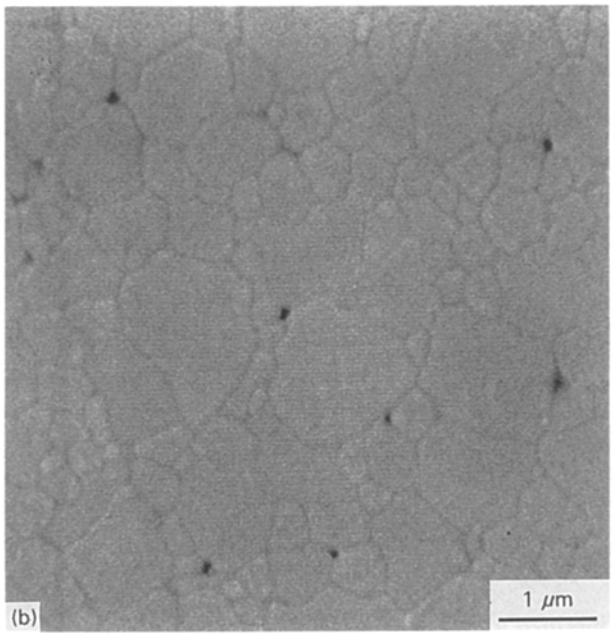

alumina content the inhibitor effect was slowed as a consequence of the alumina particles, coalescence. Fig. 16 shows the evolution of the zirconia grain size as a function of the alumina content for a constant sintering temperature, and Fig. 17 shows the variation of the grain size as a function of temperature. Depending on the alumina particle size to zirconia grain size ratio, the alumina particles are located at the grain boundaries or within the zirconia grains. A similar grain growth behaviour was found in the case of the coprecipitated zirconia samples; see Fig. 18.

4. Discussion

The above-described experimental results enable us to put forward some considerations on the sintering behaviour and the microstructural development of both commercial and coprecipitated zirconia samples.

For example, to better understand the densification behaviour of the zirconia powder compacts it is necessary to take into account the pore-size distributions after compaction. In this way the location of pores in intra- or inter-aggregates could be established, and the strength of the agglomerates or aggregates could also be known. Thus, from Fig. 1 and the specific surface data of the zirconia powders [18], it can be assumed that the packing capability of the zirconia coprecipitated powders is much higher than that of homogeneous commercial zirconia ones. At the compaction pressure of the present work (200 MPa) it could be assumed that the inter-agglomerate pores (> 100 nm) did not exist, and the majority of the pores would be located as intra- and inter-aggregates in the case of the commercial zirconia samples, and only as inter-aggregates in the coprecipitated zirconia powder compacts (20).

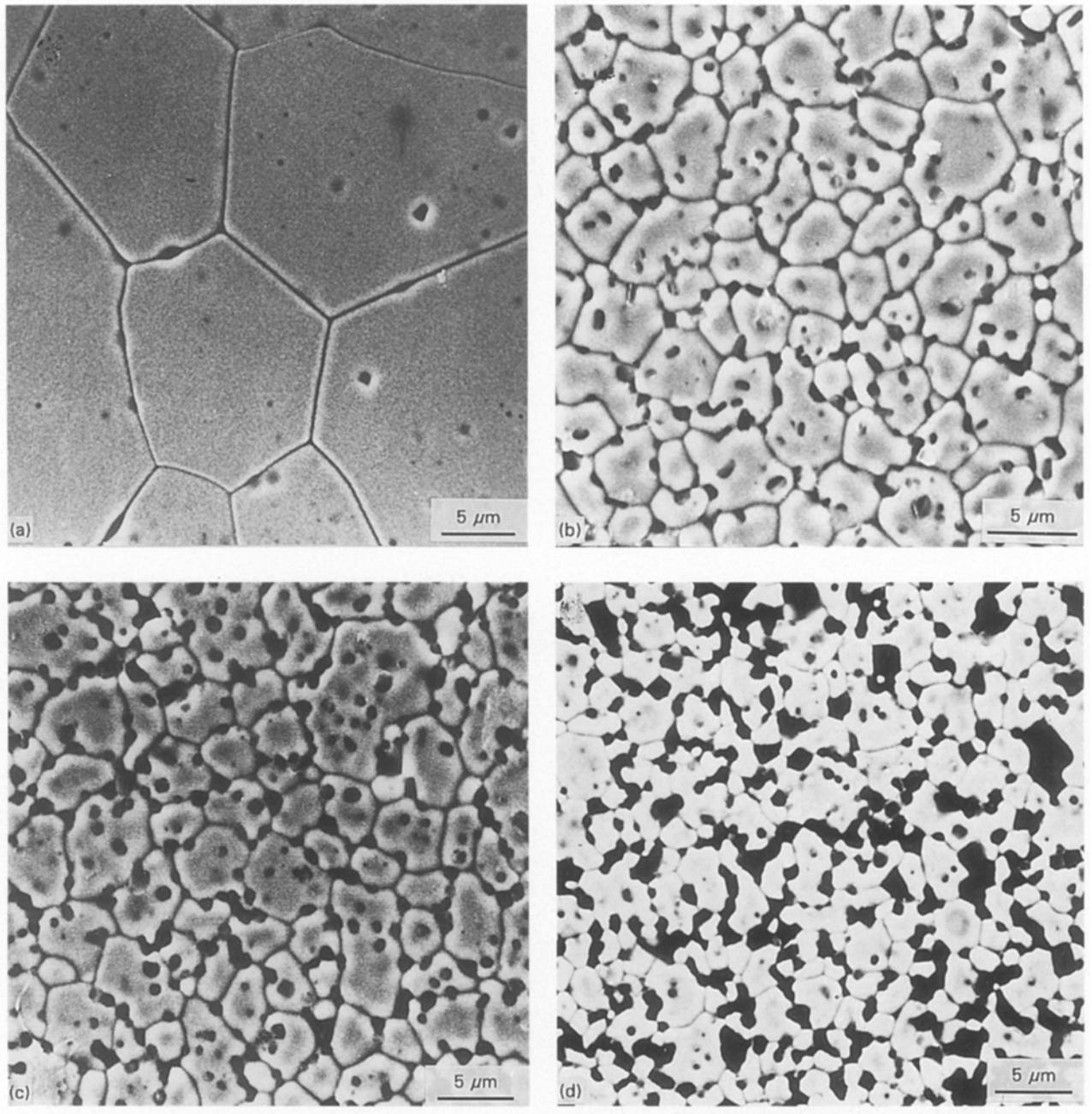

Figure 15 Grain size evolution of the Z-8Y commercial sample as a function of the alumina content. (a) 0 wt % (b) 5 wt % (c) 10 wt % and (d) 20 wt % Al_2O_3

In such a situation the elimination of intra-aggregate pores, being the first species in moving at low temperature, will produce a certain shrinkage of the aggregates and, simultaneously, as a consequence of the pores' migration towards the aggregate boundaries an increase in the pores' volume occurs. As a result of these phenomena a small expansion of the samples takes place in a narrow temperature range. The manner in which these pores, now inter-aggregate ones, are eliminated in a second step at higher temperatures will determine the final density of the sintered bodies. Thus, from Figs 6 and 7 it could be assumed that the coprecipitated zirconia samples, having only inter-aggregate pores, starts to shrink at temperatures lower ($\sim 800\,^{\circ}C$) than the commercial zirconia samples ($\geqslant 900\,^{\circ}C$). At this first stage of heating a rearrangement of the zirconia particles takes place [21] and, as the temperature rises, a local densification [22] occurs before reaching the first maximum of the shrinkage rate. As shown in Fig. 10, many dense large aggregates ($\geqslant 0.5\,\mu m$) are embedded within a fine-grained matrix. The presence of these coarse aggregates in the microstructure could be responsible for the reduction of the sintering driving force in the case of the commercial zirconia samples.

In the case of the coprecipitated zirconia samples, having a very narrow pore-size distribution with a maximum pore diameter of about 8 nm, a rapid migration of the inter-aggregate pores towards the grain boundaries was, apparently, produced at low temperature ($< 1000\,^{\circ}C$). As shown in Fig. 12, little grain growth took place, which indicates that the mobility of the pores was much higher than that of the boundaries. Above that temperature a strong shrinkage occurred, and an almost fully densified sample was obtained at about $1300\,^{\circ}C$.

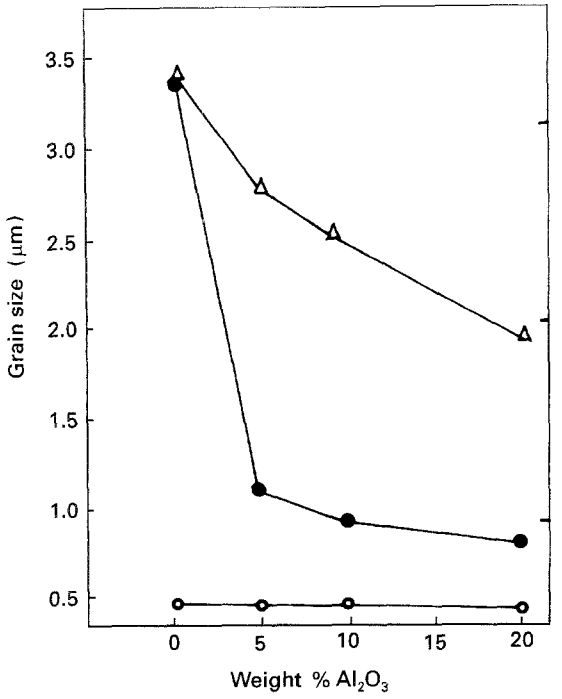

Figure 16 Variation of the grain size as a function of the alumina content in commercial zirconia samples sintered at 1400 °C. ○—○ Z-3Y; ●—● Z-6Y; △—△ Z-8Y

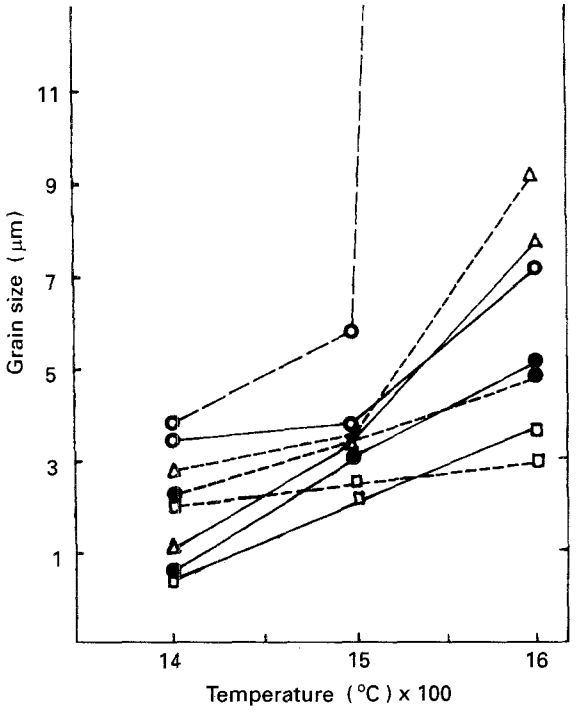

Figure 17 Influence of alumina additions on the grain growth process of Z-6Y and Z-8Y commercial zirconia samples as a function of the temperature. ○—○ Z-6Y; △—△ Z-6Y/5A; ●—● Z-6Y/10A; □—□ Z-6Y/20A; ○- - -○ Z-8Y; △- - -△ Z-8Y/5A; ●- - -● Z-8Y/10A; □- - -□ Z-8Y/20A

A grain size as small as 0.15 μm could be measured at that temperature; see Fig. 12. Above that temperature, the migration of the pores along the boundaries and a relatively high grain growth controlled the sintering up to the end of the process. A constant density of ~ 98% of theoretical density was achieved above 1400 °C for the coprecipitated samples, and no end-

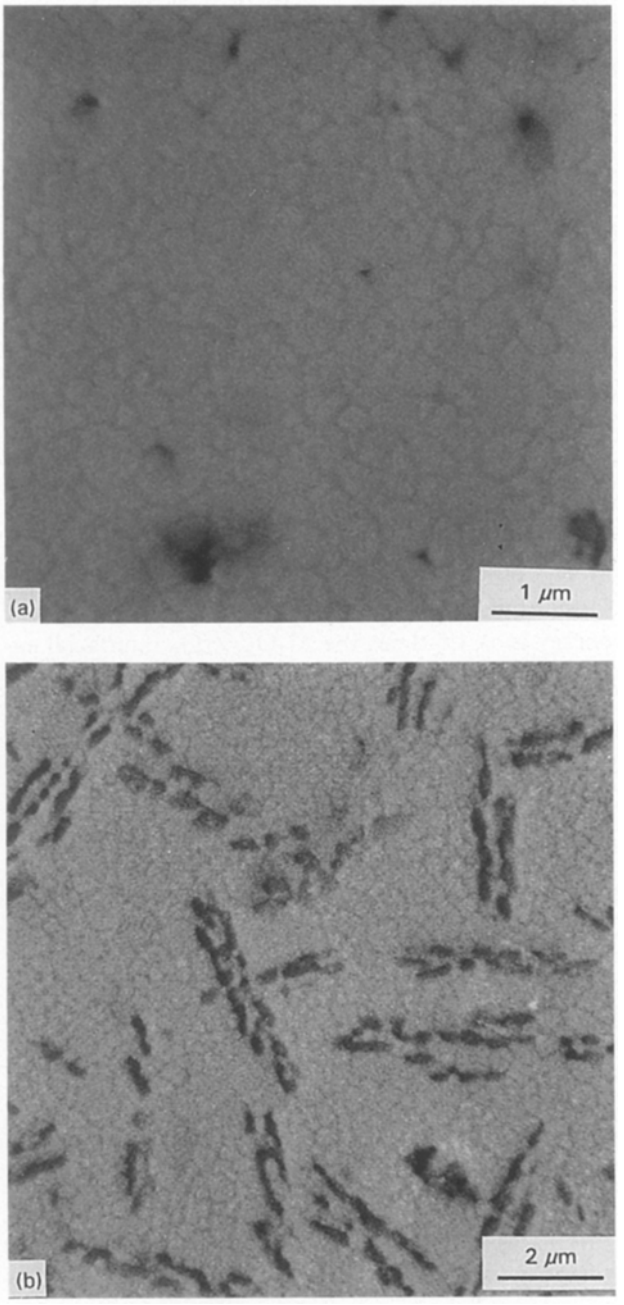

Figure 18 Influence of 10 wt % Al_2O_3 on the grain size of Z-4Y coprecipitated sample

point appeared for the commercial zirconia samples at the same temperature.

A similar phenomenon occurred in the samples containing alumina; thus while dense samples (> 99% of theoretical density) were obtained for coprecipitated zirconia compacts containing 10 wt% alumina at 1400 °C, only 94% dense samples were obtained for the same composition in the case of the commercial zirconia ones; see Figs 6a and 7. It must be emphasized that the presence of alumina increased the zirconia compacts' density (in both kinds of zirconia powders) up to a 10 wt% alumina content. Higher alumina content had a negative effect on the density of the zirconia sintered samples (see Fig. 9), as a consequence of the alumina particles' coalescence.

As reported by several authors [15, 17, 23, 24], Al_2O_3 inclusions, introduced as a second phase into

ZrO_2 powder, can, if correctly dispersed in the zirconia matrix, hinder growth of the ZrO_2 grains. As shown in Fig. 16, alumina additions do not have any effect on the grain growth process of the zirconia samples with tetragonal symmetry, i.e., in those zirconia samples in which the grain growth rate is low. However, in zirconia samples with tetragonal + cubic or single cubic structures, having a high grain growth rate of the cubic grains, the inhibitor effect of alumina in reducing the zirconia grain size was clearly observed. Thus, for a constant alumina content the zirconia grain size increased as the temperature increased, and for a constant temperature the zirconia grain size decreased as the alumina content increased. Reytkonen *et al.* [25] reported that the zirconia grain size increased as the alumina content increased in tetragonal zirconia/Al_2O_3 composites. However, Rajendran *et al.* [23] found that the zirconia grain size decreased as the alumina content increased. If, as reported by Lange and Hirlinger [15], the Al_2O_3 grain boundary energy is ~ 1.5 times the Al_2O_3/ZrO_2 interfacial energy, it could be assumed that additions of Al_2O_3 to ZrO_2 would decrease the driving force for sintering and if, as shown above, Al_2O_3 additions hinder zirconia grain growth, then its effect on the zirconia sintering would be negative. According to the results of the present work, this would be true for alumina additions higher than 10 wt %.

From the microstructural evolution observed in Figs 14 and 15 we can put forward the following considerations: (a) alumina additions, as a dispersed second phase in a zirconia matrix, hinder the zirconia grain growth process as a consequence of a competition between the higher mobility of the zirconia grain boundaries and the higher thermal expansion of the alumina particles; (b) a certain interaction must be assumed between the alumina dispersed second phase and the grain boundaries of the zirconia matrix; and (c) such an interaction strongly depends on the ratio between the zirconia grain size and that of the alumina particles. If such a ratio is at least 1.5, then the alumina particles will be trapped within the zirconia grains, and such a situation is maintained in a determined sintering temperature range. If the sintering temperature is sufficiently high ($\geqslant 1600\,^{\circ}C$) then the activity of the alumina particles moving towards the zirconia grain boundaries could be considerable and depending on the alumina content, they will coalesce there. The similarity of the alumina particles' migration towards the zirconia grain boundaries to the pores' elimination in the last step of the sintering process, as proposed by Lange *et al.* [15], is a question open to further study.

Acknowledgement

This work was supported by the Commission of the European Communities under Contract JOUE-0044C.

References

1. M. HOCH and K. M. NAIR, *Ceramurgia Int.* **2** (1976) 88.
2. M. A. C. G. VAN DE GRAAF, K. KEIZER and A. J. BURGRAAF, in "Science of ceramics", Vol. 10, edited by H. Hausner (Deutsche Keramische Gesellschaft, Berchtesgaden, Germany, 1980) p.83.
3. W. H. RHODES, *J. Amer. Ceram. Soc.* **64** (1981) 19.
4. M. A. C. G. VAN DE GRAAF and A. J. BURGRAAF, in "Advances in ceramics", Vol. 12, edited by N. Claussen, M. Ruhle and A. H. Heuer (American Ceramic Society, Columbus, Ohio, 1984) p.744.
5. P. DURAN, P. RECIO, J. R. JURADO, C. PASCUAL and C. MOURE, *J. Amer. Ceram. Soc.* **72** (1989) 2088.
6. F. F. LANGE, *J. Mater. Sci.* **17** (1982) 240.
7. T. SATO and S. SHIMADA, *J. Amer. Ceram. Soc.* **68** (1985) 256.
8. A. J. A. WINNUBST and A. J. BURGRAAF, in "Advances in ceramics", Vol. 24, Edited by S. Somiya, N. Yamamoto and H. Yanagida (American Ceramic Society, Columbus. Ohio, 1989) p.39.
9. M. T. HERNANDEZ, J. R. JURADO, P. DURAN and J. L. G. FIERRO, *J. Amer. Ceram. Soc.* **74** (1991) 1254.
10. A. J. A. WINNUBST, K. KEIZER and A. J. BURGRAAF, *J. Mater. Sci.* **18** (1983) 1958.
11. M. J. VERKERK, B. J. MIDDELHUIS and A. J. BURGRAAF, *Solid State Ion.*, **8** (1982) 159.
12. K. TSUKUMA, K. UEDA and M. SHIMADA, *J. Amer. Ceram. Soc.* **68** (1985) C-4.
13. K. TSUKUMA and M. SHIMADA, *J. Mater. Sci. Lett.* **4** (1985) 857.
14. H. YAO-YONG, G. JI-QIANG and Z. HONG-TU, *ibid.* **6** (1987) 246.
15. F. F. LANGE and M. M. HIRLINGER, *J. Amer. Ceram. Soc.* **70** (1987) 827.
16. T. SATO and M. SHIMADA, *J. Mater. Sci.* **20** (1985) 3988.
17. H. TSUBAKINO, R. NOZATO and M. YAMAMOTO, *J. Amer. Ceram. Soc.* **74** (1991) 440.
18. L. M. NAVARRO, P. RECIO and P. DURAN, *J. Mater. Sci.* This issue.
19. R. SCHÜCKHER, in "Quantitative microscopy", edited by R. T. DeHoff and F. N. Rhines (McGraw Hill, New York, 1968), p.201.
20. W. R. M. GROOTZEVERT, A. J. A. WINNUBST, G. S. A. M. THEUNISSEN and A. J. BURGRAAF, *J. Mater. Sci.* **25** (1990) 3449.
21. F. F. LANGE and M. M. HIRLINGER, *J. Amer. Ceram. Soc.* **67** (1984) 164.
22. F. F. LANG and B. I. DAVIS, in "Advances in ceramics", Vol. 12, edited by N. Claussen, M. Ruhle and A. H. Heuer (American Ceramic Society, Columbus, Ohio, 1984), p.699.
23. S. RAJENDRAN, J. DRENNAN and S. P. S. BADWAL, *J. Mater. Sci. Lett.* **6** (1987) 1431.
24. S. RAJENDRAN, M. N. SWAIN and H. J. ROSSELL, *J. Mater. Sci.* **23** (1988) 1805.
25. T. RYTKONEN, K. KESKINEN and P. LINTULA, in "Ceramic powder processing science", edited by H. Hausner, G. L. Messing and S. Hirano (Deutsche Keramische Gesellschaft, Berchtesgaden, Germany, 1988) p. 853.

Received 29 July 1994
and accepted 11 August 1994